ChemPubSoc Europe

DOI: 10.1002/cplu.201700051

CHEMPLUSCHEM Full Papers

Unsymmetrically Substituted Donor–π–Acceptor-Type 5,15-Diazaporphyrin Sensitizers: Synthesis, Optical and Photovoltaic Properties

Satoshi Omomo,[b] Yukihiro Tsuji,[c] Kenichi Sugiura,[c] Tomohiro Higashino,[c] Haruyuki Nakano,[d] Hiroshi Imahori,*[c, e] and Yoshihiro Matano*[a]

The first examples of unsymmetrical β-substituted donor–π–acceptor (D–π–A)-type 5,15-diazaporphyrin (DAP) sensitizers with both *p*-aminophenyl and *p*-carboxyphenyl groups at their peripheral 3-, 7-, 13-, and/or 17-positions have been synthesized for use in dye-sensitized solar cells (DSSCs). UV/Vis absorption and emission spectroscopy, electrochemical measurements, and DFT calculations revealed that these D–π–A dyes exhibit high light-harvesting properties over the whole visible range because of the intrinsic charge-transfer character of their electronic transitions. The cell performances of TiO_2-based DSSCs fabricated with the newly prepared DAP derivatives were evaluated under standard AM1.5 conditions. Among the four dyes examined, 13,17-bis(*p*-carboxyphenyl)-3,7-bis[*p*-(*N*,*N*-dimethylamino)phenyl]-DAP showed the highest power conversion efficiency (2.0%), which was 20 times larger than that obtained with 3-(*p*-carboxyphenyl)-DAP. These results show that the DAP chromophore could be used as the electron-accepting π unit in various types of functional dyes.

Introduction

Donor–π–acceptor (D–π–A)-type porphyrin derivatives have attracted considerable attention as functional dyes in the fields of dye-sensitized solar cells (DSSCs) and nonlinear optics (NLO) because they have intrinsically narrow HOMO–LUMO gaps and polarized excited states with a large charge-transfer (CT) character.[1–3] For example, DSSCs composed of TiO_2 and a D–π–A-type porphyrin, such as **SM315**,[1f] exhibit high power conversion efficiencies (PCEs), whereas acetylene-linked D–π–A-type porphyrins, such as **P1**,[3a] show strong second-order NLO activity and have been used as dyes for second-harmonic generation imaging (Figure 1). In DSSCs, the D–π–A structure is indispensable for acceleration of charge injection from the excited state of the dye to the conduction band (CB) of TiO_2, as well as

[a] *Prof. Dr. Y. Matano*
Department of Chemistry, Faculty of Science
Niigata University, Nishi-ku, Niigata
950-2181 (Japan)
E-mail: matano@chem.sc.niigata-u.ac.jp

[b] *S. Omomo*
Department of Fundamental Sciences
Graduate School of Science and Technology
Niigata University, Nishi-ku, Niigata
950-2181 (Japan)

[c] *Y. Tsuji, K. Sugiura, Dr. T. Higashino, Prof. Dr. H. Imahori*
Department of Molecular Engineering
Graduate School of Engineering, Kyoto University
Nishikyo-ku, Kyoto 615-8510 (Japan)

[d] *Prof. Dr. H. Nakano*
Department of Chemistry, Graduate School of Science
Kyushu University, Nishi-ku, Fukuoka 819-0395 (Japan)

[e] *Prof. Dr. H. Imahori*
Institute for Integrated Cell-Material Sciences (WPI-iCeMS)
Kyoto University, Nishikyo-ku, Kyoto 615-8510 (Japan)
E-mail: imahori@scl.kyoto-u.ac.jp

Supporting information (including experimental details) and the ORCID identification number(s) for the author(s) of this article can be found under http://dx.doi.org/10.1002/cplu.201700051.

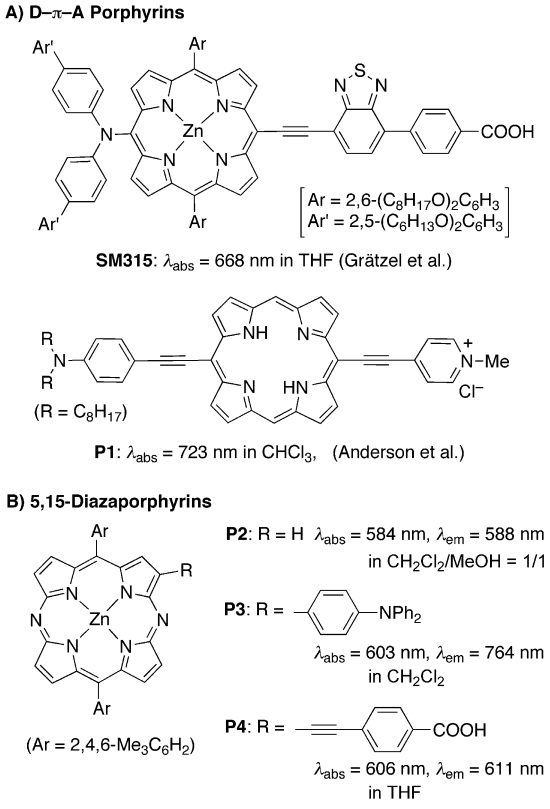

Figure 1. Structures of porphyrins and diazaporphyrins discussed herein. λ_{abs} = absorption maximum of the lowest-energy excitation, λ_{em} = emission maximum.

for suppression of charge recombination from the CB to the resulting dye radical cation.[1c,r]

In general, D–π–A-type porphyrins contain donor and acceptor moieties at the *meso*- and/or β positions.[1–3] In addition, an acetylene spacer is often inserted between the porphyrin and D/A units, as in the structures of **SM315** and **P1**, to extend π conjugation and improve the light-harvesting ability in the long-wavelength visible region. However, this type of molecular design usually requires multistep synthetic reactions and may restrict the development of easily accessible porphyrin-based dyes. In this context, the design of new chromophores that have a large CT character and good light-harvesting properties, but do not contain an additional acetylene unit, is intriguing.

In contrast to porphyrins, which have intrinsic D_{4h} symmetry, 5,15-diazaporphyrin (DAP) has D_{2h} symmetry and characteristic optical and electrochemical properties derived from 1) the nondegenerate HOMO/HOMO−1 and LUMO/LUMO+1, and 2) the low-lying LUMO of the π system.[4] Most importantly, DAP exhibits a more intense Q band than that of porphyrins owing to the symmetry-allowed HOMO–LUMO electronic transition.[4,5] We have recently established convenient methods for the synthesis and peripheral functionalization of 10,20-dimesityl-DAPs (mesityl = 2,4,6-trimethylphenyl), and revealed that introducing electron-rich substituents, such as aminophenyl, thienyl, or porphyrinyl groups, into one of the β positions of the DAP ring provides the entire π system with a large CT character.[5–7] For example, the absorption and emission bands of the zinc(II) complex of 3-[*p*-(*N*,*N*-diphenylamino)phenyl]-DAP (**P3**) were considerably redshifted compared with the corresponding bands of reference ZnDAP compound **P2** (Figure 1). The large Stokes shift of **P3**, as well as its solvatochromic behavior in solution, strongly suggested that the DAP chromophore acted as the electron-accepting π unit when an electron-donating substituent was introduced into the β position of the DAP ring.

In 2013, we reported the first example of a DAP-based DSSC, in which **P4** was used as a sensitizer (Figure 1).[8] Unfortunately, the PCE of this **P4**-based DSSC was very low (0.08%), not only because of the small driving force for electron injection from the excited state of **P4** to the CB of TiO_2, but also owing to the insufficient light-harvesting ability in the long-wavelength visible region. To use DAP derivatives as sensitizers for DSSCs, it is therefore necessary to raise the energy levels of their excited states and further narrow the HOMO–LUMO gaps of their π systems. We envisioned that these prerequisites could be simply achieved by introducing strongly electron-donating *p*-aminophenyl groups into the β positions of the DAP ring. Herein, we report the first examples of D–π–A-type DAP dyes, in which two or four of the β positions were substituted with *p*-aminophenyl (*p*-$R_2NC_6H_4$; R = Ph, Me) and *p*-carboxyphenyl groups as the donor and anchor units, respectively.[9] These dyes were prepared by sequential bromination and cross-coupling reactions, and their structure–property relationships were studied by UV/Vis absorption and emission spectroscopy, electrochemical measurements, and DFT calculations. Furthermore, DSSCs based on the new DAP dyes were fabricated and their cell performances were evaluated under standard AM1.5 conditions.

Results and Discussion

The syntheses of the β-functionalized DAPs are illustrated in Schemes 1 and 2. Reference DAP dye **2**, which contains no electron-donating group, was obtained by alkaline hydrolysis of ester **1**.[6a] Reaction of **1** with NBS in $CHCl_3$ at reflux afforded three regioisomers of β-bromo-DAP **3**. The R_f value of one regioisomer (R_f = 0.22; CH_2Cl_2/AcOEt = 100/1) was different from the R_f values of the others (each, R_f = 0.40; CH_2Cl_2/AcOEt = 100/1). On the basis of their R_f values, the more polar regioisomer (R_f = 0.22) was assigned to **3-*syn***, and the less polar, inseparable regioisomers (R_f = 0.40) were assigned to **3-*anti***. Suzuki–Miyaura cross-coupling of **3-*anti*** with *p*-(*N*,*N*-diphenylamino)-phenylboronic acid in the presence of K_2CO_3 and catalytic amounts of $Pd(OAc)_2$ and CyJohnPhos in 1,4-dioxane–water at 80 °C afforded **4** as a mixture of two regioisomers. Alkaline hydrolysis of esters **4** gave corresponding carboxylic acids **5**. The UV/Vis absorption spectrum of the mixture of regioisomers of

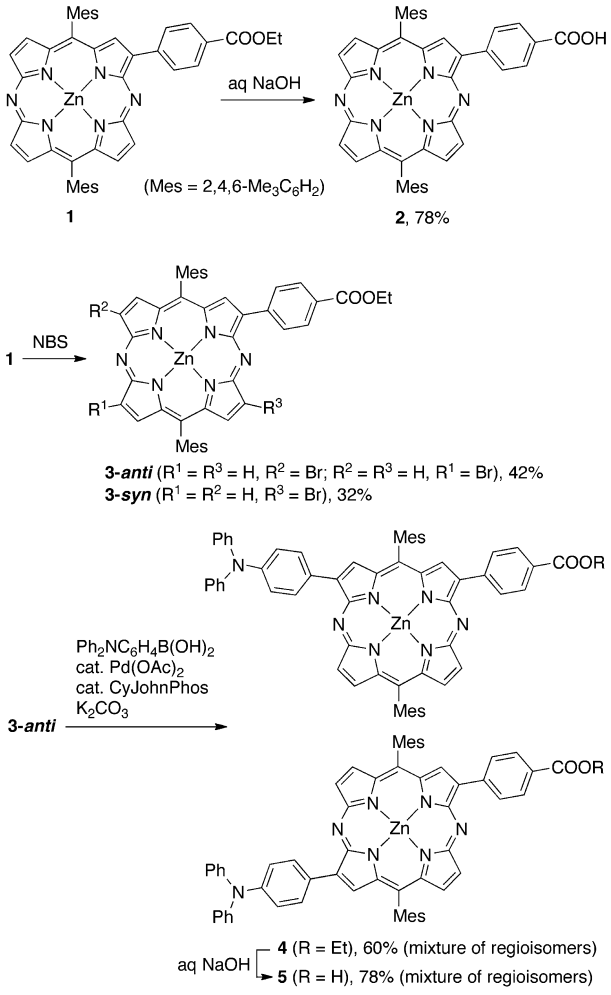

Scheme 1. Synthesis of **2**–**5**. NBS = *N*-bromosuccinimide, CyJohnPhos = 2-(dicyclohexylphosphino)biphenyl.

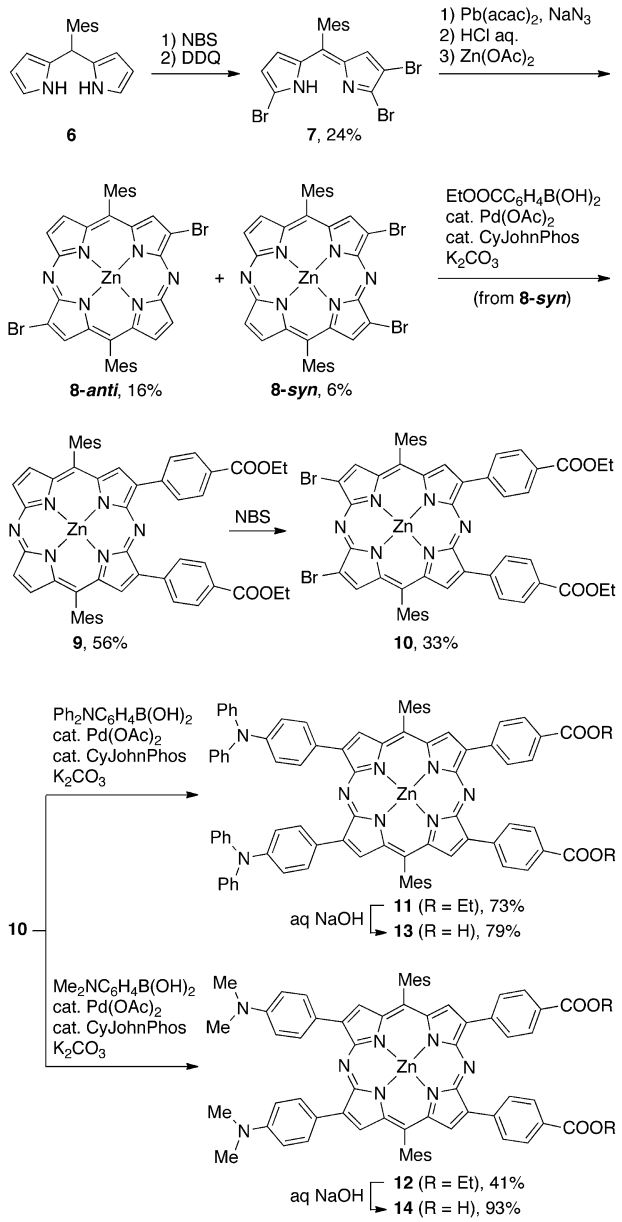

Scheme 2. Synthesis of **7**–**14**. DDQ = 2,3-dichloro-5,6-dicyano-1,4-benzoquinone, acac = acetylacetone.

4 in CH_2Cl_2 showed a Q band at $\lambda_{max} = 619$ nm, which was red-shifted compared with that of **1** ($\lambda_{max} = 596$ nm).

Next, we synthesized 3,7,13,17-tetraaryl-DAPs **11**–**14** (Scheme 2). Reaction of **7**,[10] which was available in one step from **6** and NBS, with NaN_3 and $Pb(acac)_2$ in *n*-propanol at reflux afforded two regioisomers of dibromo-DAPs as their lead(II) complexes. Demetalation of the crude lead(II) complexes, followed by insertion of zinc(II) ions into the resulting free bases, gave 3,7-dibromo-DAP **8-*syn*** and 3,13-dibromo-DAP **8-*anti*** in 6 and 16% yield, respectively, based on the amount of starting material **7**.[5b] These regioisomers had different R_f values and were successfully separated from each other by column chromatography on silica gel. Suzuki–Miyaura cross-coupling of **8-*syn*** with *p*-ethoxycarbonylphenylboronic acid gave 3,7-diaryl-DAP **9**. The *syn* stereochemistry of **9** was confirmed by preliminary X-ray crystallographic results, although the quality of the diffraction data was not at a publishable level. Bromination of **9** with NBS proceeded regioselectively to yield **10**, which underwent Suzuki–Miyaura cross-coupling with *p*-(*N*,*N*-diphenylamino)- and *p*-(*N*,*N*-dimethylamino)phenylboronic acids to give **11** and **12**, respectively. Alkaline hydrolysis of the ester groups of **11** and **12** afforded the corresponding carboxylic acids **13** and **14**, respectively.

The UV/Vis absorption and fluorescence spectra of **1**, **4**, **11**, and **12** in CH_2Cl_2 are shown in Figure 2 and Figure S1 in the Supporting Information. The spectra of the D–π–A-type DAPs

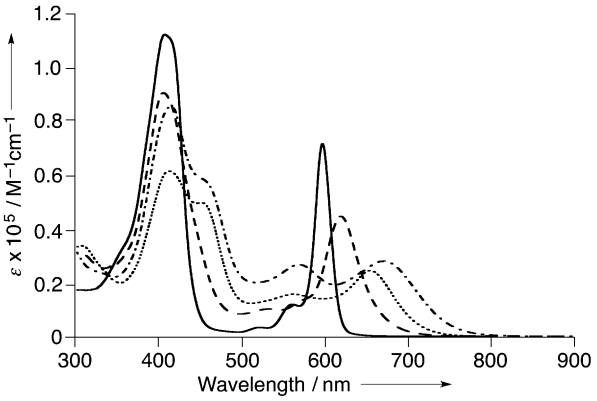

Figure 2. UV/Vis absorption spectra of **1** (——), **4** (– – –), **11** (••••), and **12** (–•–•) in CH_2Cl_2.

4, **11**, and **12** contained broad Q bands with absorption maxima (λ_{abs}) at 619, 654, and 670 nm, respectively, and broad emission bands with emission maxima (λ_{em}) at 772, 783, and 805 nm, respectively. Introduction of aminophenyl groups at the periphery considerably improved the light-harvesting ability of the DAP π systems in the long-wavelength region ($\Delta\lambda_{abs} = 23$ (**4** vs. **1**), 44 (**11** vs. **9**), and 60 nm (**12** vs. **9**); Figure S2 in the Supporting Information). From the intersections of the absorption and fluorescence spectra, the optical HOMO–LUMO gaps (ΔE_{H-L}) of **4**, **11**, and **12** were determined to be 1.85, 1.76, and 1.69 eV, respectively. Furthermore, the large Stokes shifts observed for **4**, **11**, and **12**, as well as their solvatochromic behavior in solutions of toluene, THF, CH_3CN, $CHCl_3$, CH_2Cl_2, and DMF, suggest that the β-aminophenyl groups have a critical impact on the CT character of the entire π system (Table S1 and Figure S3 in the Supporting Information). Lippert–Mataga plots for these D–π–A dyes have large slopes ($\Delta\nu\Delta f = 6.4\times10^3$ (**4**), 5.9×10^3 (**11**), and 4.7×10^3 cm^{-1} (**12**)), which implies that their HOMO–LUMO electronic transitions provide intrinsically high CT character in the excited states.[11] The spectral features of carboxylic acids **5**, **13**, and **14** (Figure S4 in the Supporting Information) were almost identical to those of the corresponding esters. Notably, D–π–A-type 3,7,13,17-tetraaryl-DAPs **11**–**14** were able to absorb almost all visible light. The λ_{abs} values of **4**, **11**, and **12** were considerably larger than those of D–π–A-type porphyrin analogues, such as **HKK-4**[1g] and **ZnPH2**[2a] (Figure 3).

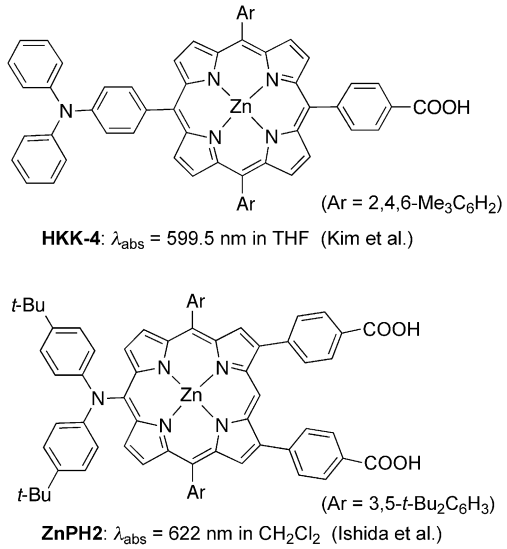

Figure 3. Structures of **HKK-4** and **ZnPH2**.

To obtain further insight into the origin of the CT character and the structures of **13** and **14**, we conducted DFT and time-dependent (TD) DFT calculations on model compounds **13-m** and **14-m**, in which the *meso*-mesityl groups were replaced by phenyl groups (Figure 4 and Table S2 in the Supporting Information). In each model, the β-aryl groups lean towards the DAP π plane to a large extent, and the torsion angles at the inter-ring bonds (27.6–30.3° for **13-m**, 25.4–30.2° for **14-m**) are close to those observed in the X-ray crystal structure of 3,7,13,17-tetraphenyl-DAP (16.2–34.6°).[5a] The inter-ring bond lengths between the β-aryl groups and the DAP ring (1.464–1.467 Å for **13-m**, 1.461–1.467 Å for **14-m**) are appreciably shorter than those between the *meso*-phenyl groups and the DAP ring (1.499 Å); this reflects the reduced single-bond character of the C_β–C_{aryl} bonds. It is therefore likely that the β-aryl and DAP rings in **13-m** and **14-m** are effectively π conjugated. As shown in Figure 4, the HOMO and HOMO−1 are largely localized on the aminophenyl groups, whereas the LUMO, LUMO+1, HOMO−2, and HOMO−3 are distributed over the DAP ring. Two low-energy excitations (<2 eV) calculated for each model by using the TD-DFT method are dominated by the HOMO–LUMO and HOMO−1–LUMO transitions. The substantial CT character of these two excitations, from the two aminophenyl groups (donor) to the DAP ring (acceptor), generates polarized excited states. This explains the definite solvatochromism observed for structurally related D–π–A dyes **11** and **12**. In addition to the low-energy CT excitations, several intense excitations (oscillator strength >0.1) that originate from DAP-based π–π* transitions are involved in the visible region. The theoretical results for **13-m** and **14-m** qualitatively support the observed spectra of **13** and **14**, which contain broad absorption bands with several absorption maxima (Figure S4 in the Supporting Information).

To evaluate the extent of the electronic effects of the β-aryl substituents on the redox properties of the DAP π system, we measured the redox potentials of **4**, **9**, **11**, and **12** in THF with

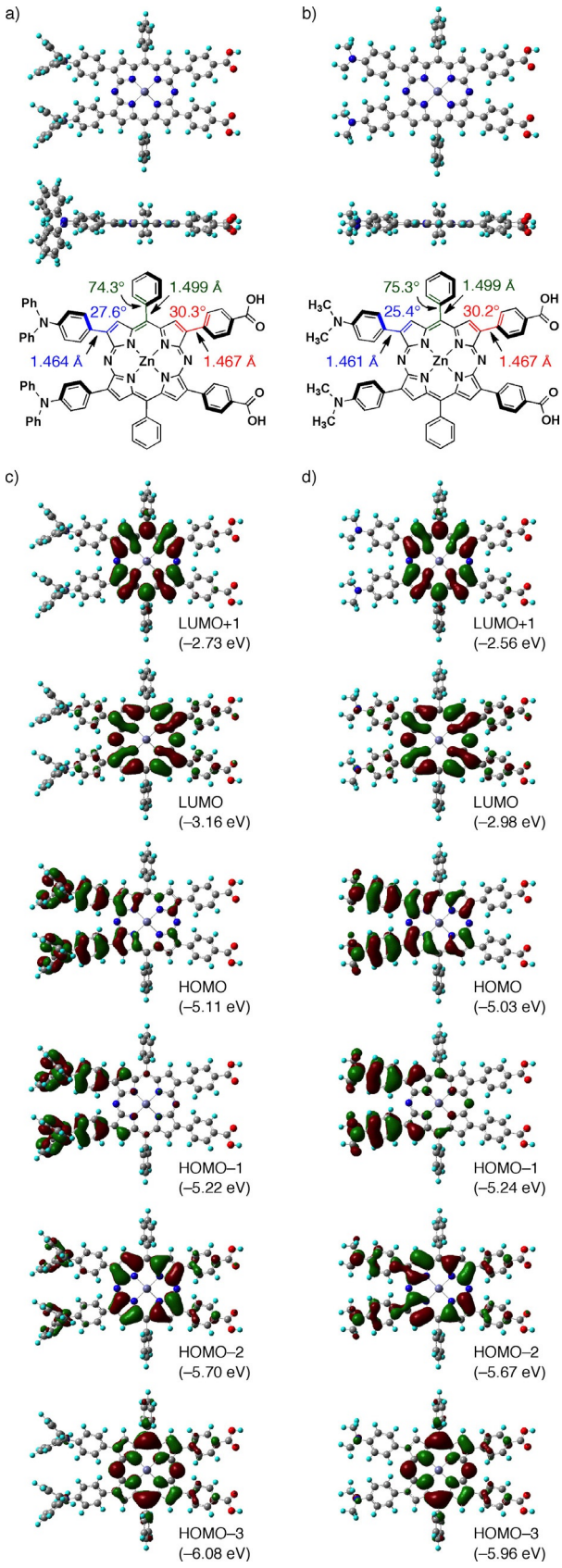

Figure 4. Top and side views of the optimized structures of a) **13-m** and b) **14-m** calculated by the DFT method. Inter-ring bond lengths and torsion angles are indicated. Selected Kohn–Sham orbitals and their energies of c) **13-m** and d) **14-m**.

Bu_4NPF_6 as the electrolyte (Table 1 and Figure S5 in the Supporting Information). The first oxidation potential (E_{ox1} versus Fc/Fc^+) of **4** (+0.50 V) was less positive than that of **1** (+0.76 V) and comparable to that of **P3** (+0.49 V).[6a] Additionally,

Table 1. Optical and electrochemical data for DAPs.

DAP	λ_{abs} [nm][a]	λ_{em} [nm][b]	E_{ox} [V][c]	$\Delta E_{0\text{-}0}$ [eV][d]
1[e]	596 (4.87)	609 (0.03)	+0.76	2.06
4	619 (4.65)	772 (0.08)	+0.50, +0.71	1.85
5	623 (4.32)	774 (0.07)	n.m.	1.85
11	654 (4.39)	783 (0.07)	+0.53, +0.76	1.76
13	654 (4.47)	784 (0.04)	n.m.	1.76
12	670 (4.45)	805 (0.03)	+0.27, +0.66	1.69
14	669 (n.m.)	802 (0.02)	n.m.	1.69
9	610 (4.79)	621 (0.02)	+0.77	2.01

[a] Absorption maxima in the range >500 nm in CH_2Cl_2. Data in parentheses are log ε. [b] Emission maxima in CH_2Cl_2. Data in parentheses are fluorescence quantum yields. [c] Oxidation potentials versus the ferrocene/ferrocenium couple (Fc/Fc^+), as determined by cyclic voltammetry (CV; in THF with 0.1 M Bu_4NPF_6). [d] Optical HOMO–LUMO gaps. [e] Data from Ref. [6a]. n.m. = not measured because of low solubility.

the E_{ox1} values of **11** (+0.53 V) and **12** (+0.27 V) were less positive than that of **9** (+0.77 V). These data indicate that the introduction of *p*-aminophenyl groups onto the β positions raises the HOMO energy levels of the DAP chromophores by 0.24–0.50 eV. The appreciable difference in the E_{ox1} values of **11** and **12** implies that the HOMO energy levels of the D–π–A dyes can also be controlled by the *N*-substituents, as suggested by DFT calculations on **13-m** and **14-m** (see above). With the optical HOMO–LUMO gaps and E_{ox1} values in hand, we next calculated the exited-state oxidation potentials (E_{ox}*) of **4**, **11**, and **12** to be −0.71, −0.59, and −0.78 eV (versus a normal hydrogen electrode (NHE)), respectively. Under our measurement conditions, the redox potentials of carboxylic acids **5**, **13**, and **14** could not be determined accurately because of their low solubility. Therefore, we estimated the driving forces for electron injection (ΔG_{inj}) from the excited states of these carboxylic acids to the CB of TiO_2 (−0.50 eV vs. NHE) from the E_{ox}* values of their ester counterparts **4**, **11**, and **12**. The ΔG_{inj} values thus estimated are in the order **11** (−0.09 eV) > **4** (−0.21 eV) > **12** (−0.28 eV).

Finally, we fabricated DSSCs by using new DAP dyes **2**, **5**, **13**, and **14**, and examined their cell performances under standard AM1.5 conditions to reveal the effects of the β substituents on the PCE. The DAP-modified TiO_2 (DAP/TiO_2) electrodes were prepared by immersing a double (for **2**, **5**) or triple (for **13**, **14**) layer TiO_2 electrode into 0.2 mM EtOH (for **2**, **5**) or EtOH/THF (for **13**, **14**) solutions of DAP at room temperature (for details, see the Experimental Section). The cell performances discussed below were obtained under optimized measurement conditions (Figures S6–S8 in the Supporting Information). The current–voltage (*I*–*V*) curves for the DSSCs are shown in Figure 5, and the short-circuit currents (J_{SC}), open-circuit voltages (V_{OC}), fill factors (FFs), and PCEs are summarized in Table 2.

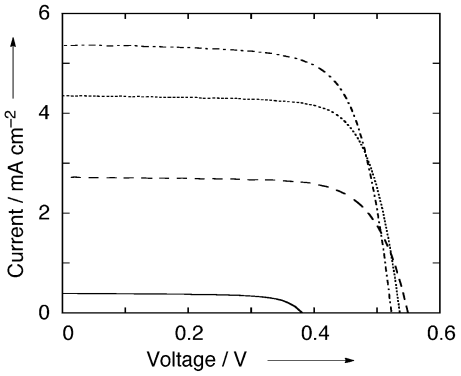

Figure 5. Photocurrent–voltage characteristics of **2**/TiO_2 (——), **5**/TiO_2 (– – –), **13**/TiO_2 (•••••), and **14**/TiO_2 (–•–•–).

Table 2. Photovoltaic parameters of DSSCs.[a]

Cell	J_{SC} [mA cm^{-2}]	V_{OC} [V]	FF	PCE [%]
2/TiO_2	0.39	0.38	0.69	0.10
5/TiO_2	2.71	0.55	0.72	1.1
13/TiO_2	4.35	0.54	0.74	1.7
14/TiO_2	5.35	0.52	0.72	2.0

[a] Measured under white-light illumination (AM1.5, 100 mW cm^{-2}).

As expected, the introduction of aminophenyl groups at the periphery of the DAP ring considerably improved the cell performances of the DAP/TiO_2 electrodes; the PCE values increased in the order **2**/TiO_2 (0.10) < **5**/TiO_2 (1.1) < **13**/TiO_2 (1.7) < **14**/TiO_2 (2.0). The effect of the β substituent on the J_{SC} value was greater than its effect on the V_{OC} and FF values. As a result, the difference in PCE values among the four cells stems mostly from the difference in their J_{SC} values. The spectral features of the photocurrent action spectra of the four cells (Figure 6a) match well with those of the absorption spectra of the corresponding DAP dyes adsorbed on TiO_2 (Figure 6b). The incident photon-to-current efficiency (IPCE) values of the **5**/TiO_2, **13**/TiO_2, and **14**/TiO_2 cells were considerably larger than those of the **2**/TiO_2 cell in all wavelength regions; this suggests that the D–π–A structure is indispensable for the achievement of high J_{SC} values.

The IPCE values of cells fabricated by using the D–π–A dyes increased in the order **5**/TiO_2 < **13**/TiO_2 < **14**/TiO_2 (Figure 6a), which agrees with the order of their absorptivities (Figure 6b). The IPCE is divided into three components: light-harvesting efficiency (LHE), quantum yield of electron injection from the dye-excited singlet state to the CB of the TiO_2 electrode, and charge collection efficiency.[12] The driving force for electron injection in the **13**/TiO_2 cell seems to be smaller than that for the **5**/TiO_2 cell. Therefore, the marked difference in the IPCE values of these two cells is probably attributed to the higher LHE and/or charge collection efficiency of **13**/TiO_2 compared with those of **5**/TiO_2. In contrast, the difference in the IPCE values of the **13**/TiO_2 and **14**/TiO_2 cells can be attributed to different LHE values and/or driving forces for the electron injec-

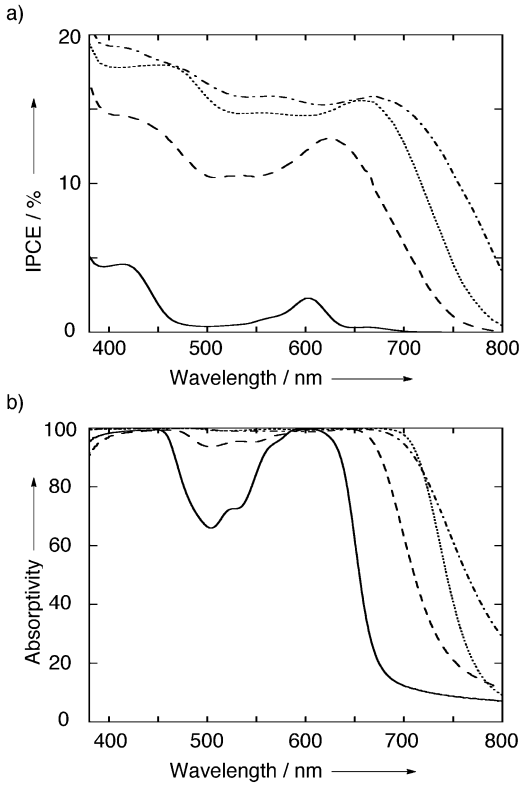

Figure 6. a) Photocurrent action and b) UV/Vis absorption spectra of **2**/TiO_2 (——), **5**/TiO_2 (– – –), **13**/TiO_2 (••••), and **14**/TiO_2 (–•–•) electrodes.

tion process. The PCEs of the **13**/TiO_2 and **14**/TiO_2 cells are smaller than those of the cells containing structurally related D–π–A-type porphyrin dyes **HKK-4** (2.7%) and **ZnPH2** (2.9–3.8%), although the lowest-energy absorption bands of **13** and **14** are redshifted compared with those of **HKK-4** and **ZnPH2**. This result may be due to the rather small ΔG_{inj} values of DAP dyes **11** and **12** compared with those of the porphyrin dyes (−0.55 eV for **HKK-4**; −0.42 eV for **ZnPH2**).[1g,2a]

Conclusion

We have studied the synthesis, structure, and optical and electrochemical properties of D–π–A-type DAP dyes, in which two or four of the β positions were unsymmetrically substituted with *p*-aminophenyl and *p*-carboxyphenyl groups, and applied them in DSSCs. The new DAPs were successfully prepared by sequential bromination and cross-coupling reactions in a few steps from the appropriate DAP precursors, and their structure–property relationships were revealed by UV/Vis absorption and emission spectroscopy, CV, and DFT calculations. The D–π–A-type DAPs displayed markedly redshifted absorption bands in the low-energy visible region; these shifts were attributed to CT transitions from the high-lying HOMO/HOMO−1 on the β-aminophenyl groups to the low-lying LUMO on the DAP ring. Notably, the 3,7-bis(*p*-aminophenyl)-13,17-bis(*p*-carboxyphenyl)-DAPs exhibited considerably higher DSSC performances than that of 3-(*p*-carboxyphenyl)-DAP. Although the observed PCEs are not yet satisfactory in terms of application of these compounds, the present results clearly show that the DAP chromophore could be used as the electron-accepting π unit in various D–π–A-type functional dyes. Further studies on DAP-based dyes, which are now underway in our laboratory, should provide new insight into the development of azaporphyrin-based materials.

Experimental Section

General

All melting points were recorded on a Yazawa micro melting point apparatus and are uncorrected. ^{1}H NMR spectra were recorded on a Varian 400 or 700 MHz spectrometer by using $CDCl_3$ or CD_2Cl_2 as solvents. Chemical shifts are reported in ppm as relative values versus tetramethylsilane. HRMS results were obtained on a Thermo Fisher Scientific EXACTIVE spectrometer. UV/Vis absorption spectra were measured at room temperature on a JASCO V-530 spectrometer. Electrochemical measurements were performed at room temperature on a CH Instruments model 650E electrochemical workstation by using a glassy carbon working electrode, a platinum wire counter electrode, and an Ag/Ag^+ (0.01 M $AgNO_3$, 0.1 M Bu_4NPF_6 (MeCN)) reference electrode. The scan rate was 60 mV s^{-1} and the potentials were calibrated with Fc/Fc^+ (0.64 V vs. NHE). Compound **1** was prepared according to reported procedures.[6a] Other chemicals and solvents were of reagent-grade quality and used without further purification, unless otherwise noted. TLC was performed with Alt. 5554 DC-Alufolien Kieselgel 60 F254 (Merck) plates, and preparative column chromatography was performed by using Silica Gel 60 (spherical, neutrality; Nacalai tesque). All reactions were performed under an argon or nitrogen atmosphere. The synthetic procedures and characterization data of new compounds are described below.

Synthesis

Compound 2: A mixture of **1** (29.8 mg, 0.0392 mmol), NaOH (558 mg, 13.9 mmol), MeOH (30 mL), THF (30 mL), and water (6 mL) was stirred at reflux temperature. After 11.5 h, the solvent was removed under reduced pressure. CH_2Cl_2 and a 3.5% aqueous solution of HCl were added to the solid residue, and the mixture was shaken vigorously. The organic phase was separated, dried over Na_2SO_4, and evaporated under reduced pressure to leave a solid residue, which was then reprecipitated from CH_2Cl_2/MeOH to give **2** as a green solid (22.6 mg, 0.0309 mmol, 78%). M.p. >300 °C; R_f (CH_2Cl_2/AcOEt/MeOH = 3/1/1): 0.85; ^{1}H NMR (400 MHz, CD_2Cl_2/CD_3OD): δ = 1.78 (s, 6H; *o*-Me), 1.81 (s, 6H; *o*-Me), 2.55 (s, 3H; *p*-Me), 2.56 (s, 3H; *p*-Me), 7.25 (s, 2H; *m*-Mes), 7.27 (s, 2H; *m*-Mes), 8.30 (d, *J* = 8.4 Hz, 2H; C_6H_4COOH), 8.60 (d, *J* = 4.8 Hz, 1H; pyrrole-β), 8.74 (d, *J* = 4.8 Hz, 1H; pyrrole-β), 8.75 (d, *J* = 4.8 Hz, 1H; pyrrole-β), 8.78 (s, 1H; pyrrole-β), 8.85 (d, *J* = 8.4 Hz, 2H; C_6H_4COOH), 9.01 (d, *J* = 4.8 Hz, 1H; pyrrole-β), 9.02 (d, *J* = 4.8 Hz, 1H; pyrrole-β), 9.15 ppm (d, *J* = 4.8 Hz, 1H; pyrrole-β); COO*H* proton was not observed; HRMS (ESI): *m/z* calcd for $C_{43}H_{35}N_6O_2Zn$: 731.2107 $[M+H]^+$; found: 731.2094.

Compound 3: NBS (12.7 mg, 0.071 mmol) was added to a solution of **1** (54.8 mg, 0.072 mmol) in $CHCl_3$ (15 mL), and stirred at reflux. After 15.5 h, the solvent was removed under reduced pressure. The residue was purified by column chromatography on silica gel with CH_2Cl_2/AcOEt/pyridine = 100/1/1 as eluents. The green fraction (R_f = 0.40; CH_2Cl_2/AcOEt = 100/1) was collected, concentrated, and

reprecipitated from CH_2Cl_2/MeOH to give a mixture of **3-*anti*** and dibrominated-**1** (34.5 mg, **3-*anti***/Br_2-**1** = 1:0.3; 42% yield for **3-*anti*** determined by NMR spectroscopy). A mixture of **3-*syn*** (R_f = 0.22; CH_2Cl_2/AcOEt = 100/1) and **1** was obtained as a green fraction (27.5 mg, **3-*syn***:**1** = 2:1; 32% yield for **3-*syn*** determined by NMR spectroscopy). Crude **3-*anti*** was used for the synthesis of **4** without further purification. **3-*anti***: m.p. > 300 °C; ^{1}H NMR (700 MHz, CD_2Cl_2): δ = 1.45 (t×2, J = 7.0 Hz, 3H×2; $COOCH_2CH_3$), 1.84 (s×2, 6H×2; *o*-Me), 1.86 (s×2, 6H×2; *o*-Me), 2.64 (s×2, 3H×2; *p*-Me), 2.66 (s×2, 3H×2; *p*-Me), 4.38 (q, J = 7.0 Hz, 2H×2; $COOCH_2CH_3$), 7.31 (s×2, 2H×2; *m*-Mes), 7.33 (s×2, 2H×2; *m*-Mes), 8.28 (d×2, J = 7.7 Hz, 2H×2; C_6H_4COOEt), 8.84–8.90 (m, 3H×2; pyrrole-β), 9.00–9.05 (m×2, 3H×2; pyrrole-β + C_6H_4COOEt), 9.27–9.32 ppm (m×2, 2H×2; pyrrole-β).

Compound 4: Compound **3-*anti*** (34.5 mg, 0.030 mmol; a mixture with 0.009 mmol of Br_2-**1**), $Pd(OAc)_2$ (1.7 mg, 0.0076 mmol), Cy-JohnPhos (5.6 mg, 0.016 mmol), K_2CO_3 (17.8 mg, 0.129 mmol), *p*-(*N*,*N*-diphenylamino)phenylboronic acid (59.3 mg, 0.205 mmol), 1,4-dioxane (6 mL), and distilled water (0.6 mL) were heated at 80 °C. After 4 h, CH_2Cl_2 and water were added, and the combined organic extracts were separated, washed with brine, dried over Na_2SO_4, and concentrated under reduced pressure to leave a solid residue, which was then purified by column chromatography on silica gel with CH_2Cl_2 as an eluent. The green fraction (R_f = 0.36; CH_2Cl_2) was collected, concentrated, and reprecipitated from CH_2Cl_2/MeOH to give **4** as a green solid (18.1 mg, 0.018 mmol, 60%). M.p. > 300 °C; UV/Vis (CH_2Cl_2): λ_{max} (log ε) = 404 (4.96), 619 nm (4.65); ^{1}H NMR (700 MHz, CD_2Cl_2): δ = 1.49 (t×2, J = 7.4 Hz, 3H×2; $COOCH_2CH_3$), 1.86–1.91 (s×4, 6H×4; *o*-Me), 2.64–2.65 (s×4, 3H×4; *p*-Me), 4.46–4.49 (q×2, J = 7.4 Hz, 2H×2; $COOCH_2CH_3$), 7.13 (t×2, J = 7.7 Hz, 2H×2; *p*-Ph), 7.28 (d×2, J = 7.7 Hz, 4H×2; *o*-Ph), 7.32–7.35 (s×4, 2H×4; *m*-Mes), 7.37 (pseudo-t×2, J = 7.7 Hz, 4H×2; *m*-Ph), 7.41 (d×2, J = 9.1 Hz, 2H×2; $C_6H_4NPh_2$), 8.38 (d×2, J = 8.4 Hz, 2H×2; C_6H_4COOEt), 8.76–8.77 (m×2, 2H×2; pyrrole-β), 8.79–8.80 (s×2, 1H×2; pyrrole-β), 8.85–8.87 (m×2, 2H×2; $C_6H_4NPh_2$), 8.97 (s×2, 1H×2; pyrrole-β), 9.04–9.06 (d×2, J = 8.4 Hz, 2H×2; C_6H_4COOEt), 9.18–9.19 (d×2, J = 4.2 Hz, 1H×2; pyrrole-β), 9.20–9.23 ppm (d×2, J = 4.2 Hz, 1H×2; pyrrole-β); HRMS (ESI): *m*/*z* calcd for $C_{63}H_{52}N_7O_2Zn$: 1002.3468 $[M+H]^+$; found: 1002.3454.

Compound 5: A mixture of **4** (17.1 mg, 0.017 mmol), NaOH (302 mg, 7.56 mmol), MeOH (15 mL), THF (15 mL), and water (3 mL) was stirred at reflux. After 5.5 h, the solvent was removed under reduced pressure. CH_2Cl_2 and a 3.5% aqueous solution of HCl were added to the solid residue, and the mixture was shaken vigorously. The organic phase was separated, dried over Na_2SO_4, and evaporated under reduced pressure to leave a solid residue, which was then reprecipitated from CH_2Cl_2/MeOH to give **5** as a green solid (13.0 mg, 0.0133 mmol, 78%). M.p. > 300 °C; UV/Vis (CH_2Cl_2): λ_{max} (log ε) = 400 (4.67), 623 nm (4.32); R_f (hexane/AcOEt = 5/2): 0.18; ^{1}H NMR (700 MHz, CD_2Cl_2/CD_3OD): δ = 1.87–1.92 (s×4, 6H×4; *o*-Me), 2.64–2.65 (s×4, 3H×4; *p*-Me), 7.14 (t×2, J = 7.7 Hz, 2H×2; *p*-Ph), 7.28 (d×2, J = 7.7 Hz, 4H×2; *o*-Ph), 7.32–7.35 (s×4, 2H×4; *m*-Mes), 7.37 (pseudo-t×2, J = 7.7 Hz, 4H×2; *m*-Ph), 7.42 (d×2, J = 8.4 Hz, 2H×2; $C_6H_4NPh_2$), 8.40 (d×2, J = 8.4 Hz, 2H×2; C_6H_4COOEt), 8.76–8.80 (m×2, 2H×2; pyrrole-β), 8.94–8.95 (s×2, 1H×2; pyrrole-β), 8.96–9.00 (m×2, 2H×2; $C_6H_4NPh_2$), 8.97 (s×2, 1H×2; pyrrole-β), 9.02–9.04 (d×2, J = 8.4 Hz, 2H×2; C_6H_4COOEt), 9.17–9.19 (d×2, J = 4.2 Hz, 1H×2; pyrrole-β), 9.20–9.23 ppm (d×2, J = 4.2 Hz, 1H×2; pyrrole-β); *COOH* proton was not observed; HRMS (ESI): *m*/*z* calcd for $C_{61}H_{48}N_7O_2Zn$: 974.3131 $[M+H]^+$; found: 974.3140.

Compound 7[10]: 5-Mesityldipyrromethane (2.893 g, 10.9 mmol) was taken in dry THF (160 mL) and cooled to −78 °C. NBS (5.843 g, 32.8 mmol) was added in three portions over 1 h. After 3 h, a solution of DDQ (2.842 g, 12.7 mmol) in THF (40 mL) was added dropwise over 10 min. After 1 h, the reaction mixture was warmed to room temperature and then evaporated under reduced pressure to leave a solid residue, which was washed with hexane/CH_2Cl_2. The filtrate was then immediately subjected to column chromatography on silica gel with hexane as an eluent to give **7** (R_f = 0.64; hexane/CH_2Cl_2 = 5/2) as a red viscous liquid (1.325 g, 2.66 mmol, 24%). ^{1}H NMR (700 MHz, $CDCl_3$): δ = 2.06 (s, 6H; *o*-Me), 2.34 (s, 3H; *p*-Me), 6.18 (d, J = 4.2 Hz, 1H; pyrrole-β), 6.22 (d, J = 4.2 Hz, 1H; pyrrole-β), 6.48 (s, 1H; pyrrole-β), 6.91 (s, 2H; *m*-Mes), 12.13 ppm (br s, 1H; NH); ^{13}C NMR (100 MHz, $CDCl_3$): δ = 19.8, 21.1, 113.2, 116.9, 118.7, 125.4, 127.9, 130.9, 131.5, 135.2, 136.5, 138.1, 138.7, 140.9, 143.5 ppm; HRMS (ESI): *m*/*z* calcd for $C_{18}H_{16}N_2Br_3$: 496.8858 $[M+H]^+$; found: 496.8860.

Compound 8: $Pb(acac)_2$ (540 mg, 1.33 mmol) was added to a solution of **7** (1.325 g, 2.66 mmol) in *n*PrOH (190 mL), and the mixture was stirred at room temperature. After 11 h, sodium azide (1.558 g, 24.0 mmol) was added, and the resulting mixture was heated at reflux for 32.5 h. After **7** was consumed, the solvent was removed under reduced pressure. CH_2Cl_2 and water were added to the reaction mixture, and the organic phase was separated, washed with water, dried over Na_2SO_4, and evaporated under reduced pressure to leave a solid residue. CH_2Cl_2 and a 3.5% aqueous solution of HCl were added to the residue, and the mixture was shaken vigorously. The organic phase was separated, washed with a saturated aqueous solution of $NaHCO_3$, dried over Na_2SO_4, and evaporated under reduced pressure to leave a solid residue, which was then reprecipitated from CH_2Cl_2/MeOH. A mixture of the resulting black solid, $Zn(OAc)_2$ (786 mg, 4.28 mmol), $CHCl_3$ (50 mL), and MeOH (50 mL) was stirred at reflux temperature. After 16 h, the solvent was removed under reduced pressure. CH_2Cl_2 and water were added to the reaction mixture, and the organic phase was separated, washed with water, dried over Na_2SO_4, and evaporated under reduced pressure to leave a solid residue, which was then purified by column chromatography on silica gel with CH_2Cl_2/AcOEt/pyridine = 100/1/1 as eluents. One violet fraction (R_f = 0.38 in CH_2Cl_2/AcOEt/pyridine = 100/1/1) was collected, concentrated, and reprecipitated from CH_2Cl_2/MeOH to give **8-*syn*** as a violet solid (65.7 mg, 0.085 mmol, 6%). Crude **8-*syn*** was used for the synthesis of **9** without further purification. The other violet fraction (R_f = 0.61 in CH_2Cl_2/AcOEt/pyridine = 100/1/1) was also collected, concentrated, and reprecipitated from CH_2Cl_2/MeOH to give **8-*anti*** as a violet solid (160.6 mg, 0.209 mmol, 16%). **8-*syn***: m.p. > 300 °C; R_f (CH_2Cl_2/AcOEt = 100/1): 0.38; ^{1}H NMR (400 MHz, $CDCl_3$/[D_5]pyridine): δ = 1.79 (s, 12H; *o*-Me), 2.63 (s, 6H; *p*-Me), 7.29 (s, 4H; *m*-Mes), 8.79 (d, J = 4.6 Hz, 2H; pyrrole-β), 8.81 (s, 2H; pyrrole-β), 9.21 ppm (d, J = 4.6 Hz, 2H; pyrrole-β); HRMS (ESI): *m*/*z* calcd for $C_{36}H_{29}Br_2N_6Zn$: 767.0106 $[M+H]^+$; found: 767.0095.

Compound 9: A mixture of **8-*syn*** (60.5 mg, 0.079 mmol), $Pd(OAc)_2$ (3.0 mg, 0.013 mmol), CyJohnPhos (10.9 mg, 0.031 mmol), K_2CO_3 (34.0 mg, 0.246 mmol), *p*-ethoxycarbonylphenylboronic acid (151.0 mg, 0.778 mmol), 1,4-dioxane (15 mL), and distilled water (1.5 mL) was heated at 80 °C. After 2.5 h, CH_2Cl_2 and water were added, and the combined organic extracts were separated, washed with brine, dried over Na_2SO_4, and concentrated under reduced pressure to leave a solid residue, which was then purified by column chromatography on silica gel with CH_2Cl_2/AcOEt/pyridine = 100/1/1 as eluents. The green fraction (R_f = 0.15 in CH_2Cl_2/AcOEt = 100/1) was collected, concentrated, and reprecipitated from CH_2Cl_2/MeOH to give a mixture of **9** and **1** as a black solid

(45.1 mg; **9**:**1** = 1:0.15; 56% yield determined by NMR spectroscopy). Crude product **9** was used for the synthesis of **11** without further purification. Compound **9** could be separate from **1** by repeated column chromatography (CH_2Cl_2/AcOEt/pyridine = 100/1/1), and the spectral data of **9** were measured by using this purified sample. M.p. 245–250 °C (decomp); R_f (CH_2Cl_2/AcOEt = 100/1): 0.15; UV/Vis (CH_2Cl_2): λ_{max} ($\log\varepsilon$) = 425 (5.03), 610 nm (4.79); ^{1}H NMR (700 MHz, $CDCl_3$): δ = 1.49 (t, J = 7.0 Hz, 6H; $COOCH_2CH_3$), 1.83 (s, 12H; *o*-Me), 2.64 (s, 6H; *p*-Me), 4.49 (q, J = 7.0 Hz, 4H; $COOCH_2CH_3$), 7.29 (s, 4H; *m*-Mes), 8.33 (d, J = 8.4 Hz, 4H; C_6H_4COOEt), 8.76 (d, J = 4.8 Hz, 2H; pyrrole-β), 8.98 (s, 2H; pyrrole-β), 9.01 (d, J = 8.4 Hz, 4H; C_6H_4COOEt), 9.18 ppm (d, J = 4.8 Hz, 2H; pyrrole-β); HRMS (ESI): *m/z* calcd for $C_{54}H_{47}N_6O_4Zn$: 907.2945 $[M+H]^+$; found: 907.2932.

Compound 10: NBS (8.3 mg, 0.047 mmol) was added to a solution of **9** (20.2 mg, 0.020 mmol; a mixture with 0.003 mmol of **1**) in $CHCl_3$ (5 mL), and the resulting mixture was stirred at reflux. After 14.5 h, the solvent was removed under reduced pressure. The residue was purified by column chromatography on silica gel with CH_2Cl_2/AcOEt = 100/1 as eluents. The green fraction (R_f = 0.31; CH_2Cl_2/AcOEt = 100/1) was collected, concentrated, and reprecipitated from CH_2Cl_2/MeOH to give a mixture of **10** and tribrominated **9** (1:0.15) as a black solid (8.2 mg; **10**/Br_3-**9** = 1:0.15; 33% yield determined by NMR spectroscopy). Crude product **10** was used for the synthesis of **11** without further purification. M.p. > 300 °C; ^{1}H NMR (700 MHz, $CDCl_3$): δ = 1.44 (t, J = 7.0 Hz, 6H; $COOCH_2CH_3$), 1.87 (s, 12H; *o*-Me), 2.67 (s, 6H; *p*-Me), 4.33 (q, J = 7.0 Hz, 4H; $COOCH_2CH_3$), 7.34 (s, 4H; *m*-Mes), 8.13 (d, J = 8.1 Hz, 4H; C_6H_4COOEt), 8.84 (s, 2H; pyrrole-β), 8.91 (d, J = 8.1 Hz, 4H; C_6H_4COOEt), 8.98 ppm (s, 2H; pyrrole-β); HRMS (ESI): *m/z* calcd for $C_{54}H_{45}Br_2N_6O_4Zn$: 1063.1155 $[M+H]^+$; found: 1063.1151.

Compounds 11 and 12: A mixture of **10** (19.2 mg, 0.016 mmol; a mixture with 0.002 mmol of Br_3-**9**), $Pd(OAc)_2$ (0.8 mg, 0.004 mmol), CyJohnPhos (2.6 mg, 0.0074 mmol), K_2CO_3 (7.6 mg, 0.055 mmol), *p*-(*N*,*N*-diphenylamino)phenylboronic acid (52.1 mg, 0.180 mmol), 1,4-dioxane (5 mL), and distilled water (0.5 mL) was heated at 80 °C. After 3 h, CH_2Cl_2 and water were added, and the combined organic extracts were separated, washed with brine, dried over Na_2SO_4, and concentrated under reduced pressure to leave a solid residue, which was then purified by column chromatography on silica gel with CH_2Cl_2/AcOEt (100/5) as eluents. The dark-green fraction (R_f = 0.67; CH_2Cl_2/AcOEt = 100/1) was collected, concentrated, and reprecipitated from CH_2Cl_2/MeOH to give **11** as a black solid (16.3 mg, 0.012 mmol, 73%). Compound **12** (R_f = 0.74; CH_2Cl_2/AcOEt = 100/1) was synthesized in 41% yield from **10**, according to a similar procedure with *p*-(*N*,*N*-dimethylamino)phenylboronic acid as the coupling partner. **11**: m.p. > 300 °C; UV/Vis (CH_2Cl_2): λ_{max} ($\log\varepsilon$) = 410 (4.79), 654 nm (4.47); ^{1}H NMR (700 MHz, $CDCl_3$/[D_5]pyridine): δ = 1.52 (t, J = 7.7 Hz, 6H; $COOCH_2CH_3$), 1.89 (s, 12H; *o*-Me), 2.66 (s, 6H; *p*-Me), 4.51 (q, J = 7.7 Hz, 4H; $COOCH_2CH_3$), 7.01 (m, 4H; *p*-Ph), 7.20 (m, 8H; *o*-Ph), 7.23 (m, 8H; *m*-Ph), 7.31 (s, 4H; *m*-Mes), 7.34 (d, J = 8.4 Hz, 4H; $C_6H_4NPh_2$), 8.35 (d, J = 8.4 Hz, 4H; C_6H_4COOEt), 8.77 (s, 2H; pyrrole-β), 8.85 (d, J = 8.4 Hz, 4H; $C_6H_4NPh_2$), 8.94 (s, 2H; pyrrole-β), 9.02 ppm (d, J = 8.4 Hz, 4H; C_6H_4COOEt); HRMS (ESI): *m/z* calcd for $C_{90}H_{73}N_8O_4Zn$: 1393.5041 $[M+H]^+$; found: 1393.5042. **12**: m.p. > 300 °C; UV/Vis (CH_2Cl_2): λ_{max} ($\log\varepsilon$) = 413 (4.93), 568 (4.43), 670 nm (4.45); ^{1}H NMR (700 MHz, $CDCl_3$): δ = 1.52 (t, J = 7.0 Hz, 6H; $COOCH_2CH_3$), 1.93 (s, 12H; *o*-Me), 2.70 (s, 6H; *p*-Me), 3.00 (s, 12H; NMe_2), 4.51 (q, J = 7.0 Hz, 4H; $COOCH_2CH_3$), 6.94 (d, J = 8.4 Hz, 4H; $C_6H_4NMe_2$), 7.34 (s, 4H; *m*-Mes), 8.35 (d, J = 8.4 Hz, 4H; C_6H_4COOEt), 8.73 (s, 2H; pyrrole-β), 8.93 (d, J = 8.4 Hz, 4H; $C_6H_4NMe_2$), 8.95 (s, 2H; pyrrole-β), 9.01 ppm (d, J = 8.4 Hz, 4H; C_6H_4COOEt); HRMS (ESI): *m/z* calcd for $C_{70}H_{65}N_8O_4Zn$: 1145.4415 $[M+H]^+$; found: 1145.4432.

Compounds 13 and 14: A mixture of **11** (11.1 mg, 0.0080 mmol), NaOH (101 mg, 2.53 mmol), MeOH (7 mL), THF (7 mL), and water (1.5 mL) was stirred at reflux. After 4 h, the solvent was removed under reduced pressure. CH_2Cl_2 and a 3.5% aqueous solution of HCl were added to the solid residue, and the mixture was shaken vigorously. The organic phase was separated, dried over Na_2SO_4, and evaporated under reduced pressure to leave a solid residue, which was then reprecipitated from CH_2Cl_2/MeOH to give **13** as a green solid (8.4 mg, 0.0063 mmol, 79%). Compound **14** was synthesized in 93% yield from **12**, according to a similar procedure. **13**: m.p. > 300 °C; UV/Vis (CH_2Cl_2): λ_{max} ($\log\varepsilon$) = 411 (4.88), 654 nm (4.47); ^{1}H NMR (700 MHz, $CDCl_3$/CD_3OD): δ = 1.93 (s, 12H; *o*-Me), 2.67 (s, 6H; *p*-Me), 7.03 (m, 4H; *p*-Ph), 7.21 (m, 8H; *o*-Ph), 7.25 (m, 8H; *m*-Ph), 7.33 (s, 4H; *m*-Mes), 7.35 (d, J = 8.4 Hz, 4H; $C_6H_4NPh_2$), 8.38 (d, J = 8.4 Hz, 4H; C_6H_4COOEt), 8.78 (s, 2H; pyrrole-β), 8.84 (d, J = 8.4 Hz, 4H; $C_6H_4NPh_2$), 8.95 (s, 2H; pyrrole-β), 9.01 ppm (d, J = 8.4 Hz, 4H; C_6H_4COOEt); COO*H* proton was not observed; HRMS (ESI): *m/z* calcd for $C_{86}H_{66}N_8O_4Zn$: 1337.4415 $[M+H]^+$; found: 1337.4410. **14**: m.p. > 300 °C; ^{1}H NMR (700 MHz, [D_6]acetone): δ = 1.98 (s, 12H; *o*-Me), 2.67 (s, 6H; *p*-Me), 3.20 (s, 12H; NMe_2), 7.13 (d, J = 8.4 Hz, 4H; $C_6H_4NMe_2$), 7.40 (s, 4H; *m*-Mes), 8.40 (d, J = 8.4 Hz, 4H; C_6H_4COOEt), 8.70 (s, 2H; pyrrole-β), 8.94 (d, J = 8.4 Hz, 4H; $C_6H_4NMe_2$), 9.01 (s, 2H; pyrrole-β), 9.14 ppm (d, J = 8.4 Hz, 4H; C_6H_4COOEt); COO*H* proton was not observed; HRMS (ESI): *m/z* calcd for $C_{65}H_{57}N_8O_4Zn$: 1089.3789 $[M+H]^+$; found: 1089.3771.

DFT calculations

The geometry of **14-m** was optimized by using the DFT method. The 6-311G(d,p) basis set[13] was used for H, C, N, and O, and the Wachters-Hay all-electron basis set[14] supplemented with one f-function (exponent: 1.62) was used for Zn. The functional of DFT was the Becke three-parameter Lee–Yang–Parr (B3LYP) exchange-correlation functional.[15] The Cartesian coordinates are summarized in Table S2 in the Supporting Information. Selected Kohn–Sham orbitals and their energies are summarized in Figure 4. All calculations were performed by using the Gaussian 09 suite of programs.[16]

Fabrication of dye-sensitized TiO_2 electrodes

The preparation of TiO_2 electrodes and the fabrication of the sealed cells for photovoltaic measurements were performed according to procedures reported in the literature.[1q,17] Nanocrystalline TiO_2 particles (d = 20 nm, CCIC:PST23NR, JGC-CCIC, d = 20 nm, CCIC:PST18NR, JGC-CCIC, and d = 30 nm, CCIC:PST30NRD, JGC-CCIC) were used as the transparent layer of the photoanode, whereas sub-microcrystalline TiO_2 particles (d = 400 nm, CCIC:PST400C, JGC-CCIC) were used as the light-scattering layers of the photoanode. The working electrode was prepared by cleaning fluorine-doped tin oxide (FTO) glass (solar 4 mm thickness, 10 Ω/□, Nippon Sheet Glass) with a solution of detergent in an ultrasonic bath for 15 min, rinsing with distilled water and ethanol, and drying in air. The electrode was subjected to UV/O_3 irradiation for 18 min, immersed in a 40 mM freshly prepared aqueous solution of $TiCl_4$ at 70 °C for 30 min, washed with distilled water and ethanol, and dried. Nanocrystalline TiO_2 paste was coated onto the FTO glass by screen printing, followed by standing in a clean box for a few minutes, and drying at 125 °C for 6 min; this process was repeated to attain a final thickness of 12 μm (12 μm thickness of

PST23NR TiO_2 layer) for **2** and **5**, or 10 μm (8 μm thickness of PST18NR TiO_2 layer and 2 μm thickness of PST30NRD TiO_2 layer) for **13** and **14**. A layer of 4 μm sub-microcrystalline TiO_2 paste was deposited in the same fashion as the nanocrystalline layer. These thickness conditions were initially optimized by using YD2. Finally, the electrode was heated under an air flow at 325 °C for 5 min, 375 °C for 5 min, 450 °C for 15 min, and 500 °C for 15 min. The thickness of the films was determined by using a surface profiler (SURFCOM 130A, ACCRETECH). The size of the TiO_2 film was 0.16 cm^2 (4×4 mm). The TiO_2 electrode was then subjected to immersion into a 40 mM freshly prepared aqueous solution of $TiCl_4$ at 70 °C for 25 min before rinsing with distilled water and ethanol, and drying in air. The electrode was sintered at 500 °C for 30 min, cooled to 70 °C, and immersed into the dye solution at 25 °C in the dark for the prescribed times. The TiO_2 electrode was immersed into 0.20 mM solutions of diazaporphyrin in ethanol (for **2** and **5**) or ethanol/THF (v/v = 4/1; for **13** and **14**).

The counter electrode was prepared by drilling a small hole in FTO glass (solar 1 mm thickness, 10 Ω/□, Nippon Sheet Glass), rinsing with distilled water and ethanol, followed by treatment with 0.1 M HCl in 2-propanol by using an ultrasonic bath for 15 min. After heating in air for 15 min at 400 °C, platinum was deposited on the FTO glass by coating with a drop of a solution of H_2PtCl_6 (2 mg in 1 mL of ethanol) twice. Finally, the FTO glass was heated at 400 °C for 15 min to obtain the counter Pt electrode.

A sandwich cell was prepared by using the dye-anchored TiO_2 film as a working electrode and a counter Pt electrode, which were assembled with a hot-melt ionomer film Surlyn polymer gasket (DuPont, 50 μm), and the superimposed electrodes were tightly held and heated at 110 °C to seal the two electrodes. The aperture of the Surlyn frame was 2 mm larger than that of the area of the TiO_2 film, and its width was 1 mm. The hole in the counter Pt electrode was sealed by a film of Surlyn. A hole was then made in the Surlyn film covering with a needle. A drop of an electrolyte was put on the hole in the back of the counter Pt electrode. It was introduced into the cell by vacuum back-filling. Finally, the hole was sealed with Surlyn film and a cover glass (0.13–0.17 mm thickness). A solder was applied on each edge of the FTO electrodes. The electrolyte solution used was 1.0 M 1,3-dimethylimidazolium iodide, 0.03 M I_2, 0.05 M LiI, 0.10 M guanidinium thiocyanate, and 0.50 M 4-*tert*-butylpyridine in a mixture of acetonitrile and valeronitrile (85:15).

The IPCE and *I–V* performances were measured on an action spectrum measurement setup (CEP-2000RR, BUNKOUKEIKI) and a solar simulator (PEC-L10, Peccell Technologies) with a simulated sunlight of AM 1.5 (100 mW cm^{-2}), respectively. IPCE (%) = $100 \times 1240 \times i/(W_{in}\lambda)$, in which i is the photocurrent density (A cm^{-2}), W_{in} is the incident light intensity (W cm^{-2}), and λ is the excitation wavelength (nm). During photovoltaic measurements, a black mask was attached on the back of the TiO_2 electrode, except for the TiO_2 film region, to avoid scattering light. Convolution of the spectral response in the photocurrent action spectrum with the photon flux of the AM 1.5G spectrum provided the estimated J_{SC} value, which was in good agreement with the J_{SC} value obtained from the *I–V* performance measurements.

Acknowledgements

This study was supported by JSPS KAKENHI (15H00931 and 15K13762 to Y.M., 15K05392 to H.N., 25220801 to H.I.) and Research Fellow (16J07131 to S.O.) from MEXT, Japan. S.O. and Y.M. thank Prof. Mao Minoura (Rikkyo University) for X-ray analysis of ***9****.*

Conflict of interest

The authors declare no conflict of interest.

Keywords: donor–acceptor systems · dyes/pigments · electrochemistry · porphyrinoids · sensitizers

[1] For selected examples, see: a) A. Yella, H.-W. Lee, H. N. Tsao, C. Yi, A. K. Chandiran, M. K. Nazeeruddin, E. W.-G. Diau, C.-Y. Yeh, S. M. Zakeeruddin, M. Grätzel, *Science* **2011**, *334*, 629; b) T. Higashino, H. Imahori, *Dalton Trans.* **2015**, *44*, 448; c) M. Urbani, M. Gätzel, M. K. Nazeeruddin, T. Torres, *Chem. Rev.* **2014**, *114*, 12330; d) L.-L. Li, E. W.-G. Diau, *Chem. Soc. Rev.* **2013**, *42*, 291; e) H. Imahori, T. Umeyama, S. Ito, *Acc. Chem. Res.* **2009**, *42*, 1809; f) S. Mathew, A. Yella, P. Gao, R. H. Baker, B. F. E. Curchod, N. A. Astani, I. Tavernelli, U. Rothlisberger, M. K. Nazeeruddin, M. Grätzel, *Nat. Chem.* **2014**, *6*, 242; g) K. D. Seo, M. J. Lee, H. M. Song, H. S. Kang, H. K. Kim, *Dyes Pigm.* **2012**, *94*, 143; h) T. Bessho, S. M. Zakeeeruddin, C. Y. Yeh, E. W.-G. Diau, M. Grätzel, *Angew. Chem. Int. Ed.* **2010**, *49*, 6646; *Angew. Chem.* **2010**, *122*, 6796; i) Y.-C. Chang, C.-L. Wang, T.-Y. Pan, S.-H. Hong, C.-M. Lan, H.-H. Kuo, C.-F. Lo, H.-Y. Hsu, C.-Y. Lin, E. W.-G. Diau, *Chem. Commun.* **2011**, *47*, 8910; j) C.-P. Hsieh, H.-P. Lu, C.-L. Chiu, C.-W. Lee, S.-H. Chuang, C.-L. Mai, W.-N. Yen, S.-J. Hsu, E. W.-G. Diau, C.-Y. Yeh, *J. Mater. Chem.* **2010**, *20*, 1127; k) S.-L. Wu, H.-P. Lu, H.-T. Yu, S.-H. Chuang, C.-L. Chiu, C.-W. Lee, E. W.-G. Diau, C.-Y. Yeh, *Energy Environ. Sci.* **2010**, *3*, 949; l) C.-W. Lee, H.-P. Lu, C.-M. Lan, Y.-L. Huang, Y.-R. Liang, W.-N. Yen, Y.-C. Liu, Y.-S. Lin, E. W.-G. Diau, C.-Y. Yeh, *Chem. Eur. J.* **2009**, *15*, 1403; m) C.-L. Wang, C.-M. Lan, S.-H. Hong, Y.-F. Wang, T.-Y. Pan, C.-W. Chang, H.-H. Kuo, M.-Y. Kuo, E. W.-G. Diau, C.-Y. Lin, *Energy Environ. Sci.* **2012**, *5*, 6933; n) S. Mathew, H. Iijima, Y. Toude, T. Umeyama, Y. Matano, S. Ito, N. V. Tkachenko, H. Lemmetyinen, H. Imahori, *J. Phys. Chem. C* **2011**, *115*, 14415; o) W. Zhou, Z. Cao, S. Jiang, H. Huang, L. Deng, Y. Liu, P. Shen, B. Zhao, S. Tan, X. Zhang, *Org. Electron.* **2012**, *13*, 560; p) M. J. Lee, K. D. Seo, H. M. Song, M. S. Kang, Y. K. Eom, H. S. Kang, H. K. Kim, *Tetrahedron Lett.* **2011**, *52*, 3879; q) K. Kurotobi, Y. Toude, K. Kawamoto, Y. Fujimori, S. Ito, P. Chabera, V. Sundström, H. Imahori, *Chem. Eur. J.* **2013**, *19*, 17075; r) J. N. Clifford, G. Yahioglu, L. R. Milgrom, J. R. Durrant, *Chem. Commun.* **2002**, 1260.

[2] a) M. Ishida, D. Hwang, Z. Zhang, Y. J. Choi, J. Oh, V. M. Lynch, D. Y. Kim, J. L. Sessler, D. Kim, *ChemSusChem* **2015**, *8*, 2967; b) M. Ishida, S. W. Park, D. Hwang, Y. B. Koo, J. L. Sessler, D. Y. Kim, D. Kim, *J. Phys. Chem. C* **2011**, *115*, 19343; c) M. Ishida, D. Hwang, Y. B. Koo, J. Sung, D. Y. Kim, J. L. Sessler, D. Kim, *Chem. Commun.* **2013**, *49*, 9164; d) J. K. Park, H. R. Lee, J. Chen, H. Shinokubo, A. Osuka, D. Kim, *J. Phys. Chem. C* **2008**, *112*, 16691; e) G. Copley, D. Hwang, D. Kim, A. Osuka, *Angew. Chem. Int. Ed.* **2016**, *55*, 10287; *Angew. Chem.* **2016**, *128*, 10443.

[3] a) J. E. Reeve, H. A. Collins, K. D. Mey, M. M. Kohl, K. J. Thorley, O. Paulsen, K. Clays, H. L. Anderson, *J. Am. Chem. Soc.* **2009**, *131*, 2758; b) S. M. LeCours, H.-W. Guan, S. G. DiMagno, C. H. Wang, M. J. Therien, *J. Am. Chem. Soc.* **1996**, *118*, 1497; c) T. G. Zhang, Y. Zhao, I. Asselberghs, A. Persoons, K. Clays, M. J. Therien, *J. Am. Chem. Soc.* **2005**, *127*, 9710; d) T. G. Zhang, Y. Zhao, K. Song, I. Asselberghs, A. Persoons, K. Clays, M. J. Therien, *Inorg. Chem.* **2006**, *45*, 9703.

[4] For selected examples, see: a) N. Kobayashi in *The Porphyrin Handbook, Vol. 2* (Eds.: K. Kadish, K. M. Smith, R. Guilard), Academic Press, San Diego, **2000**, pp. 301 – 360; b) H. Ogata, T. Fukuda, K. Nakai, Y. Fujimura, S. Neya, P. A. Stuzhin, N. Kobayashi, *Eur. J. Inorg. Chem.* **2004**, 1621; c) N. Pan, Y. Bian, M. Yokoyama, R. Li, T. Fukuda, S. Neya, J. Jiang, N. Kobayashi, *Eur. J. Inorg. Chem.* **2008**, 5519; d) Y. Matano, *Chem. Rev.* **2017**, *ASAP*, DOI: 10.1021/acs.chemrev.6b00460.

[5] a) Y. Matano, T. Shibano, H. Nakano, H. Imahori, *Chem. Eur. J.* **2012**, *18*, 6208; b) Y. Matano, T. Shibano, H. Nakano, Y. Kimura, H. Imahori, *Inorg. Chem.* **2012**, *51*, 12879; c) Shinokubo et al. independently reported the synthesis of β-unsubstituted DAP, see: M. Horie, Y. Hayashi, S. Yamaguchi, H. Shinokubo, *Chem. Eur. J.* **2012**, *18*, 5919.

[6] a) S. Omomo, K. Furukawa, H. Nakano, Y. Matano, *J. Porphyrins Phthalocyanines* **2015**, *19*, 775; b) S. Omomo, Y. Maruyama, K. Furukawa, T. Furuyama, H. Nakano, N. Kobayashi, Y. Matano, *Chem. Eur. J.* **2015**, *21*, 2003; c) F. Abou-Chahine, D. Fujii, H. Imahori, H. Nakano, N. V. Tkachenko, Y. Matano, H. Lemmetyinen, *J. Phys. Chem. B* **2015**, *119*, 7328; d) Y. Matano, D. Fujii, T. Shibano, K. Furukawa, T. Higashino, H. Nakano, H. Imahori, *Chem. Eur. J.* **2014**, *20*, 3342.

[7] a) A. Yamaji, J.-Y. Shin, Y. Miyake, H. Shinokubo, *Angew. Chem. Int. Ed.* **2014**, *53*, 13924; *Angew. Chem.* **2014**, *126*, 14144; b) A. Yamaji, S. Hiroto, J.-Y. Shin, H. Shinokubo, *Chem. Commun.* **2013**, *49*, 5064.

[8] K. Kurotobi, K. Kawamoto, Y. Toude, Y. Fujimori, Y. Kinjo, S. Ito, Y. Matano, H. Imahori, *Chem. Lett.* **2013**, *42*, 725.

[9] DAP derivatives with two kinds of aryl substituents at two *meso* positions were reported, see: M. Yamamoto, Y. Takano, Y. Matano, K. Stranius, N. V. Tkachenko, H. Lemmetyinen, H. Imahori, *J. Phys. Chem. C* **2014**, *118*, 1808.

[10] 5-(*p*-tolyl)-2,3,8-Tribromodipyrrin was synthesized by using a similar procedure, see: V. Lakshmi, M. Ravikanth, *Eur. J. Org. Chem.* **2014**, 5757.

[11] J. R. Lakowicz, *Principles of Fluorescence Spectroscopy, 3rd ed.*, Springer, Berlin, **2006**.

[12] J. Rochford, D. Chu, A. Hagfeldt, E. Galoppini, *J. Am. Chem. Soc.* **2007**, *129*, 4655.

[13] R. Krishnan, J. S. Binkley, R. Seeger, J. A. Pople, *J. Chem. Phys.* **1980**, *72*, 650.

[14] a) A. J. H. Wachters, *J. Chem. Phys.* **1970**, *52*, 1033; b) P. J. Hay, *J. Chem. Phys.* **1977**, *66*, 4377; c) K. Raghavachari, G. W. Trucks, *J. Chem. Phys.* **1989**, *91*, 1062.

[15] a) A. D. Becke, *J. Chem. Phys.* **1993**, *98*, 5648; b) C. Lee, W. Yang, R. G. Parr, *Phys. Rev. B* **1988**, *37*, 785.

[16] Gaussian 09, Revision E.01, M. J. Frisch, G. W. Trucks, H. B. Schlegel, G. E. Scuseria, M. A. Robb, J. R. Cheeseman, G. Scalmani, V. Barone, B. Mennucci, G. A. Petersson, H. Nakatsuji, M. Caricato, X. Li, H. P. Hratchian, A. F. Izmaylov, J. Bloino, G. Zheng, J. L. Sonnenberg, M. Hada, M. Ehara, K. Toyota, R. Fukuda, J. Hasegawa, M. Ishida, T. Nakajima, Y. Honda, O. Kitao, H. Nakai, T. Vreven, J. A. Montgomery, Jr., J. E. Peralta, F. Ogliaro, M. Bearpark, J. J. Heyd, E. Brothers, K. N. Kudin, V. N. Staroverov, T. Keith, R. Kobayashi, J. Normand, K. Raghavachari, A. Rendell, J. C. Burant, S. S. Iyengar, J. Tomasi, M. Cossi, N. Rega, J. M. Millam, M. Klene, J. E. Knox, J. B. Cross, V. Bakken, C. Adamo, J. Jaramillo, R. Gomperts, R. E. Stratmann, O. Yazyev, A. J. Austin, R. Cammi, C. Pomelli, J. W. Ochterski, R. L. Martin, K. Morokuma, V. G. Zakrzewski, G. A. Voth, P. Salvador, J. J. Dannenberg, S. Dapprich, A. D. Daniels, O. Farkas, J. B. Foresman, J. V. Ortiz, J. Cioslowski, D. J. Fox, Gaussian, Inc., Wallingford CT, **2009**.

[17] S. Ito, T. N. Murakami, P. Comte, P. Liska, C. Grätzel, M. K. Nazeeruddin, M. Grätzel, *Thin Solid Films* **2008**, *516*, 4613.

Manuscript received: February 1, 2017
Accepted Article published: February 7, 2017
Final Article published: February 24, 2017